Crystallization mechanisms of a $Se_{85}Te_{15}$ glassy alloy

1996 J. Phys.: Condens. Matter 8 927

(http://iopscience.iop.org/0953-8984/8/8/005)

J. Phys.: Condens. Matter **8** (1996) 927–940. Printed in the UK

Crystallization mechanisms of a $Se_{85}Te_{15}$ glassy alloy

Y Calventus†, S Suriñach‡ and M D Baró‡§

† ETSEIT, UPC, 08222 Terrassa, Spain

‡ Departament de Física, UAB, 08193 Bellaterra, Spain

Received 21 July 1995, in final form 20 November 1995

Abstract. The coupling of calorimetric and microscopic techniques shows that the whole crystallization process of a $Se_{85}Te_{15}$ glassy alloy proceeds by two mechanisms which are called surface and bulk. These mechanisms are activated differently depending on the particular heating rate used and on the temperature of the isothermal heat treatment chosen. The nucleation frequency and growth rate are determined from reflection polarized optical microscopy analysis and a good agreement is found between these experimental results and predictions obtained by use of the classical nucleation and the normal growth theories. The relation between the apparent activation energy from the whole crystallization process which is obtained via differential scanning calorimetry and the activation energies of nucleation and growth deduced from microstructural analysis is established. A detailed discussion about the meaning of the different Avrami indexes found is presented, and discrepancies between time–temperature–transformation (T–T–T) curves built from both differential scanning calorimetry results and the nucleation frequency and growth rate fits can be explained in terms of these two different mechanisms determined.

1. Introduction

Chalcogenide semiconducting glasses have recently received attention because of their unusual and interesting properties, of importance not only for practical applications but also for gaining further understanding of physical phenomena in chalcogenide glasses. While amorphous Se has been and continues to be investigated extensively, efforts made to study and understand binary and ternary Se-based glassy alloys have been intensifying for the last decade or so (Afify 1991, 1992, Abdel-Rahim 1992, Venugopal Reddy and Bhatnagar 1992). Se and Te are isoelectronic, and when mixed form a continuous series of solid solutions. According to Grison (1951), their atomic arrangement in the crystal state consists of infinite chains of atoms spiralling around the *c* axis, the bonding between neighbouring atoms in the same chain being covalent, while the bonding between chains seems to be intermediate between metallic bond and van der Waals in character. The first structural model developed for Se–Te amorphous alloys assumes the coexistence of rings and copolymer chains according to the amorphous selenium structure (Ward 1970). But new advances on amorphous selenium structure show that it is formed by only Se_n chains, and amorphous Se–Te structure has been supposed to be mainly constituted by copolymer chains where Se and Te atoms are randomly distributed (Tamura *et al* 1991, Miyanaga *et al* 1993). The transport properties are influenced by the structural effects associated with thermally induced transitions (Mehra *et al* 1993).

§ Author to whom any correspondence should be addressed.

0953-8984/96/080927+14$19.50

Recently it has been pointed out that Se–Te alloys have some advantages over amorphous Se, as far as their use in xerography is concerned (Yang *et al* 1986). The main applications of Se–Te amorphous alloy are: (a) its great storage capacity and a very fast access to information; and (b) the chance to delete and introduce new information, but these advantages depend on material stability.

Therefore, in technical applications the thermal stability of chalcogenide glasses is a problem of fundamental interest, because the useful operating temperature range will be determined by the structural changes and eventual crystallization occurring at the operating temperature. In addition, crystallization studies are of interest in fundamental studies of the mechanisms of crystal nucleation and growth. Increasingly crystallization is being exploited as a means to produce alloys with suitable crystalline phases, morphologies and distributions. In the present work a bulk $Se_{85}Te_{15}$ glassy alloy has been chosen because it is located in the middle of the glass-forming region of the system. Its crystallization behaviour has been studied in detail using differential scanning calorimetry (DSC), reflection polarized optical microscopy (POM), x-ray diffraction (XRD) and scanning electron microscopy (SEM) techniques. Nucleation frequencies, growth rates, activation energies and the crystallization mechanism have been determined. The relation between calorimetric and microscopic results is discussed.

2. Experimental details

Bulk $Se_{85}Te_{15}$ glassy alloys were prepared by air quenching the molten alloy.

Differential scanning calorimetry (DSC) measurements were carried out in a computerized Perkin–Elmer DSC2 under a pure dynamic argon atmosphere. Specimens of about 10 mg of the sample in bulk form were sealed in standard aluminium pans and analysed using both continuous-heating and isothermal regimes. The continuous-heating experiments were carried out from room temperature to about 500 K at scan rates, β, in the range 0.62–40 K min^{-1}. The isothermal experiments were performed by heating up to the heat treatment temperatures (in the range of 365–385 K) at a rate of 320 K min^{-1}; subsequent cooling was performed at the same rate. From these experiments the crystalline fraction, α, and the transformation rate, $d\alpha/dt$, have been determined (see, for instance, Baró *et al* 1993).

To identify the structural changes, XRD investigations of the $Se_{85}Te_{15}$ powder were carried out with a Siemens D-500 diffractometer with a low-temperature camera (A.PARR.TTK) using Cu Kα radiation. The temperature range chosen went from room temperature to 460 K.

Microstructure observations of fresh fracture surfaces of partially crystallized bulk samples, with different degrees of crystallinity, were performed using a scanning electron microscope (Hitachi S-570).

Reflection polarized optical microscopy (POM) studies were done on polished bulk samples heat treated for different times at five temperatures (350, 360, 370, 380 and 390 K) using a Zeiss Axioplan microscope. Direct analysis of the optical micrographs allowed us to determine crystal sizes and number densities, as well as the fraction of crystallized material, using standard quantitative metallographic methods (Cahn and Nutting 1959). Further details on the samples preparation for microstructural studies were recently described by Calventus (1994).

3. Results

3.1. Calorimetric behaviour and crystallization kinetics

The as-quenched glasses exhibit a glass transition and an exothermic crystallization peak prior to melting. At 20 K min^{-1}, the glass transition temperature (T_g), the peak crystallization temperature (T_p) and the liquidus temperature (T_l) for the $Se_{85}Te_{15}$ in bulk form were $T_g = 341$ K, $T_p = 425$ K and $T_l = 526$ K respectively. The melting enthalpy is 6.6 kJ (g atom)$^{-1}$. The kinetic nature of both transformations is evident from their dependence upon heating rate.

The study of the crystallization kinetics was performed by combining both isothermal and continuous-heating regimes. To analyse the thermal behaviour we assumed a kinetic equation of the form

$$\frac{d\alpha}{dt} = K(T) f(\alpha) \tag{1}$$

which gives the rate of crystallization, in separate variables, as a function of the crystallized fraction, α, and of the temperature, T. Furthermore, we assumed that the kinetic factor $K(T)$, in the limited interval explored experimentally, follows an Arrhenius behaviour:

$$K(T) = K_0 \exp\left(-\frac{E_c}{RT}\right) \tag{2}$$

with E_c the apparent activation energy for crystallization and K_0 the pre-exponential factor. The apparent activation energy for the global crystallization process (E_c) was deduced from the Kissinger plot: $\ln(\beta/T_p^2)$ versus $1/T_p$ with β the heating rate and T_p the temperature of the maximum of the peak (Kissinger 1957). The result obtained for the $Se_{85}Te_{15}$ in bulk form is 100 ± 10 kJ mol^{-1}.

Table 1. Different values of the n-exponent tabulated versus the crystallized fraction, α, and for isothermal and non-isothermal tests.

Test	$n \pm 0.1$	$n \pm 0.5$	$n \pm 0.5$
Isothermal	$\alpha \leqslant 0.3$	$0.3 \leqslant \alpha \leqslant 0.6$	$0.6 \leqslant \alpha$
365 K (No 1)	1.5	1.7	2.5
370 K (No 2)	1.5	1.7	2.5
380 K (No 3)	1.5	2.0	4.0
385 K (No 4)	1.5	2.0	4.0
Non-isothermal			
0.62 K min^{-1}	1.5	2.0	4.0
1.25 K min^{-1}	1.5	2.0	4.0
2.5 K min^{-1}	1.5	2.0	3.0
5 K min^{-1}	1.5	3.0	3.0
10 K min^{-1}	2.0	3.0	3.0
20 K min^{-1}	2.0	2.5	2.5

To determine the best model that could explain the crystallization behaviour of the $Se_{85}Te_{15}$ glassy alloy, a comparison between different models, and experimental curves obtained in isothermal and continuous-heating-rate conditions has been made (Suriñach *et al* 1983). A plot of $\ln K_0 f(\alpha)$ or $\ln(d\alpha/dt)$ against $-\ln(1-\alpha)$ for isothermal tests allowed us to determine the function $f(\alpha)$. In figure 1, $\ln(d\alpha/dt)$ is plotted versus $-\ln(1-\alpha)$.

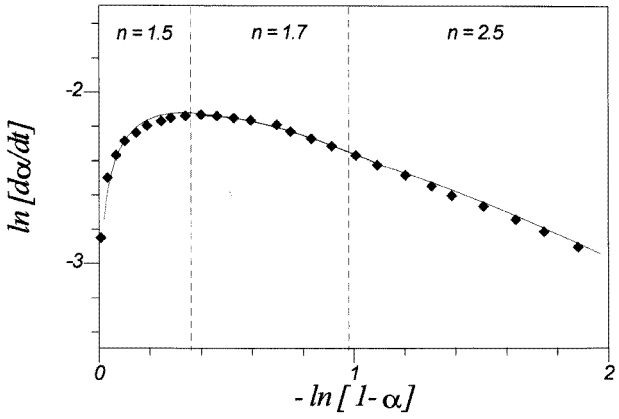

Figure 1. A plot of $\ln(\mathrm{d}\alpha/\mathrm{d}t)$ versus $-\ln(1-\alpha)$ for an isothermal test performed at 370 K.

The best fit to the experimental values is obtained by the Johnson–Mehl–Avrami–Erofe'ev (JMAE) model in which the volume fraction α transformed isothermally at a temperature T as a function of time t obeys the following equation:

$$f(\alpha) = n\,(1-\alpha)\,[-\ln(1-\alpha)]^{(n-1)/n} \tag{3}$$

where n is the JMAE exponent, and conclusions about the crystallization mechanisms can be drawn from its value. But, in our case, it is impossible to find a single value of the n-exponent that exactly reproduces all the crystallization process, which means that the crystallization process is governed by different mechanisms (Germain *et al* 1979). In this way, different sections in the latter plots, which fit to different values of n, are found. Generally speaking, surface crystallization (and at other preferential places like a hole or a fracture) and bulk crystallization will coexist. From this analysis the results obtained for the values of the exponent n are summarized in table 1.

3.2. Structural and morphological analysis

The amorphous state of the as-prepared samples was demonstrated by x-ray diffraction. The evolution as a function of temperature of the XRD patterns shows that the emerging crystalline phase reflections correspond to h.c.p. Se(Te), and on increasing the temperature the peaks become narrower and sharper until crystallization is completed. From the x-ray diffraction results the lattice parameters a and c for the $Se_{85}Te_{15}$ hexagonal structure can be calculated and the values obtained are $a = 4.45 \pm 0.01$ Å and $c = 5.06 \pm 0.01$ Å. The results are in agreement with those obtained by other authors (Grison 1951, Bordas 1977, Kotkata *et al* 1981).

Optical and scanning electron microscopy were employed to observe the type and extent of crystallization obtained after thermal treatments of the glass. Surface and bulk crystallization can be observed; in both cases crystalline nuclei develop in a spherulitic form. A surface crystallization detail can be seen in the micrograph shown in figure 2 (for the sample heat treated for 4 min at 390 K). Typical micrographs obtained by SEM and by reflection polarized optical microscopy are shown in figure 3.

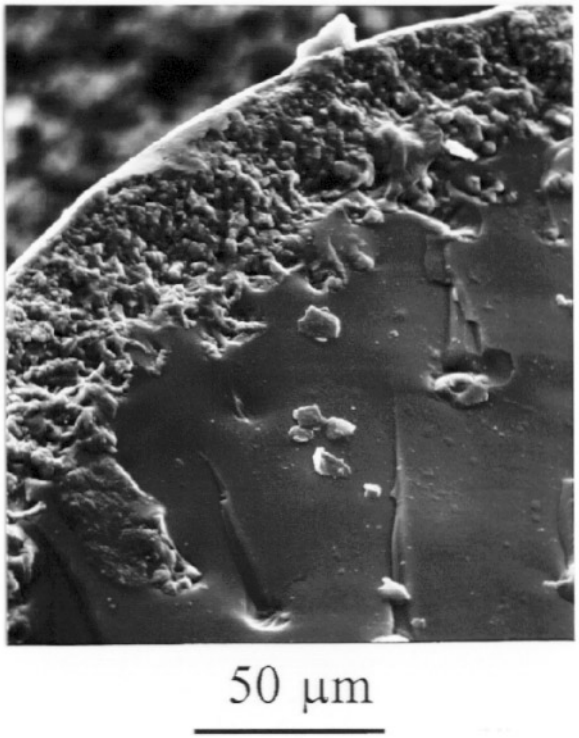

Figure 2. SEM micrograph of $Se_{85}Te_{15}$ glassy alloy heat treated at 390 K for 4 min.

3.3. Crystal growth and crystal nucleation

The growth rates of the spherulites in the bulk were evaluated from plots of the largest spherulite sizes versus heat treatment time and are shown in figure 4. It should be noted that the growth rate observed remains constant at each temperature, with an increasing growth rate at increasing temperature. This behaviour suggests a polymorphic crystallization with interphase-controlled growth (Ranganathan and von Heimendahl 1981).

Table 2. Experimental values at different temperatures for the growth rate u, and nucleation frequency I.

T (K)	u (m s^{-1})	I (m^{-3} s^{-1})
350	$1.90 \times 10^{-10} \pm 1.1 \times 10^{-11}$	$5.50 \times 10^{9} \pm 1.6 \times 10^{8}$
360	$1.25 \times 10^{-9} \pm 8.10 \times 10^{-11}$	$1.60 \times 10^{10} \pm 6 \times 10^{8}$
370	$3.62 \times 10^{-9} \pm 1.4 \times 10^{-10}$	$3.60 \times 10^{10} \pm 2.2 \times 10^{9}$
380	$1.35 \times 10^{-8} \pm 1.0 \times 10^{-9}$	$1.00 \times 10^{11} \pm 6 \times 10^{9}$
390	$3.80 \times 10^{-8} \pm 8 \times 10^{-10}$	$1.12 \times 10^{11} \pm 7 \times 10^{9}$

To obtain the number of nuclei per unit volume, N_v, the number of nuclei per unit area, N_A, taken from the picture, must be divided by the average crystal size, $\bar{\Phi}$:

$$N_v = \frac{N_A}{\bar{\Phi}}. \tag{4}$$

(*a*)

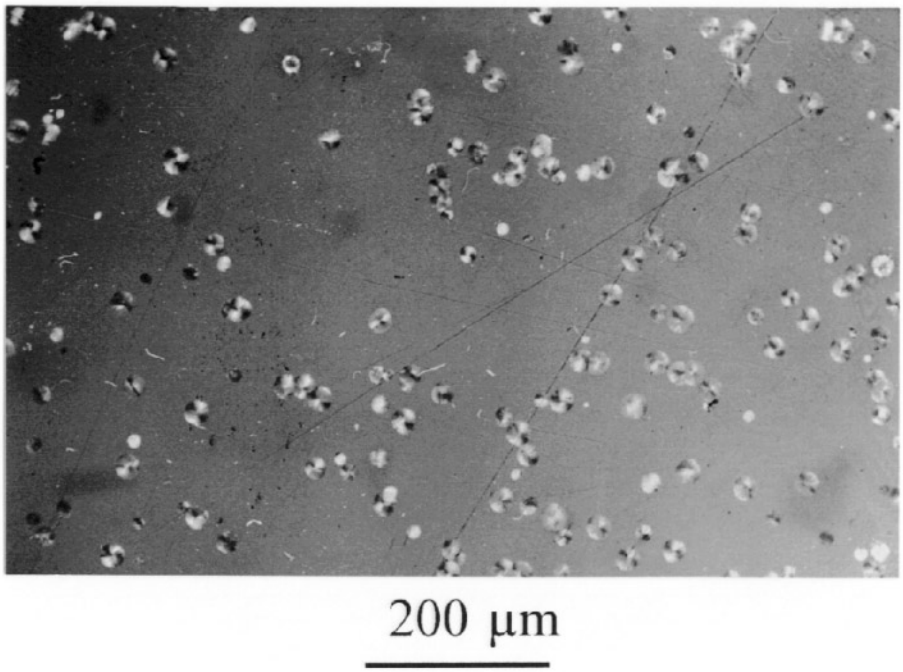

(*b*)

Figure 3. SEM and optical micrographs corresponding to a sample heat treated at 380 K for 15 min.

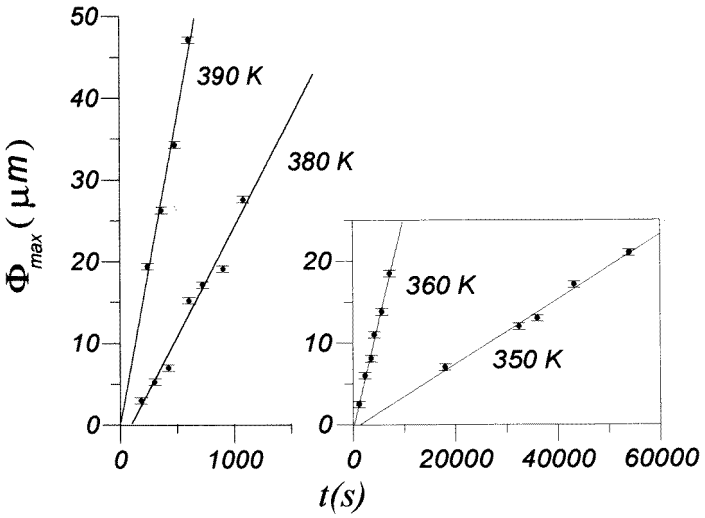

Figure 4. The growth of crystals (Φ_{max}) versus time for different isothermal heat treatments.

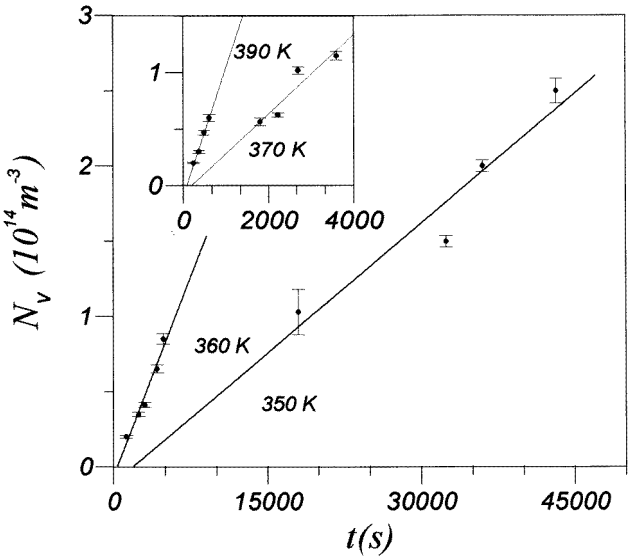

Figure 5. The number of nuclei per unit volume, N_v, versus time for different isothermal heat treatments.

On using this equation, it is assumed that the same spacing between crystals occurs in all dimensions. The nucleation frequencies, I, were evaluated from plots of the number of crystals as a function of time at each heat treatment temperature and are presented in figure 5. Constant nucleation frequencies with increasing temperature are seen only after an induction time, which decreases in value as the temperature rises. Its nature will be discussed in the next section. Experimental values of the growth rate and nucleation frequency are given in table 2.

The temperature dependence of both the nucleation frequency and the growth rate, when a broad range of temperatures is considered, is far from Arrhenian, but in a narrower range, an Arrhenius behaviour can be assumed. The activation energies for nucleation (E_N) and for growth (E_G) have been evaluated from this dependence. The values obtained are $E_N = 108 \pm 11$ kJ mol^{-1} and $E_G = 148 \pm 15$ kJ mol^{-1}, respectively (Baró *et al* 1992).

3.4. The temperature dependence of the nucleation frequency and growth rate from the classical nucleation and normal growth theories

The nucleation frequency, I, and growth rate, u, can be studied in agreement with the classical homogeneous nucleation and crystalline growth theories according to the following equations:

$$I = \frac{N_v^0 kT}{3\pi a_0^3 \gamma} \exp\left(-\frac{16\pi\sigma_g^3}{3RT(\Delta G_v^l)^2}\right) \tag{5}$$

$$u = \frac{fkT}{3\pi a_0^2 \gamma}\left(1 - \exp\left(-\frac{\Delta G_v^l}{kT}\right)\right) \tag{6}$$

where N_v^0 is the number of atoms per unit volume in the matrix (amorphous) phase, k is Boltzmann's constant, a_0 is the mean atomic diameter, f is the fraction of sites where atoms may be added preferentially, which will be taken as $f = 1$, γ is the viscosity, ΔG_v^l the Gibbs free-energy difference between the supercooled liquid and the crystal, σ is the molar free-interface enthalpy between the nucleus and the liquid, R is the universal constant of gases, and T is the absolute temperature.

In order to model the nucleation frequency and the growth rate the following input parameters were adopted. Assuming a linear dependence for the density of liquid Se and Te (Das *et al* 1972) a value of $N_v^0 = 3.08 \times 10^{28}$ m^{-3} was found and a value of $a_0 = 3 \times 10^{-10}$ m was used. We consider for the viscosity behaviour in the undercooling region a Vogel–Fulcher equation of the form

$$\gamma = \gamma_0 \exp\left(\frac{A}{T - T_0}\right) \tag{7}$$

where γ_0, A and T_0 are constants. The experimental values of the viscosity of a $Se_{85}Te_{15}$ alloy were taken from Rialland and Perron (1976). The best fit to them gives the following parameters: $\gamma_0 = 2.33 \times 10^{-2}$ N s m^{-2}, $A = 2040$ K and $T_0 = 248$ K. The validity of the fit has been checked by comparison to the temperature coefficients of the viscosity of pure Se given by Faivre and Gardissat (1986), $A = 2765$ K and $T_0 = 239$ K.

Because the nucleation frequency has an exponential dependence on ΔG_v^l, the accuracy of its estimation is often critically important when used in the analysis of nucleation phenomena. Although there has been an attempt at describing the thermodynamic functions for the Se–Te system by the Redlich–Kister polynomial method (Ghosh *et al* 1988), the results are not completely satisfactory. Taking into account that the Se–Te phase diagram system presents a great proximity between solidus and liquidus lines, we consider $Se_{85}Te_{15}$ as a monocomponent alloy, and ΔG_v^l was calculated using the expression of Thompson and Spaepen (1979):

$$\Delta G_v^l = \frac{\Delta H_m \, \Delta T}{T_m}\left(\frac{(1-\zeta)\, T_m + (1+\zeta)\, T}{T_m + T}\right) \tag{8}$$

where T_m is the melting temperature, ΔH_m is the melting enthalpy, and ζ is a parameter related to ΔC_p. A value of $\zeta = 2$ has proven to be suitable for reproducing the experimental results relating the temperature dependence of I and u.

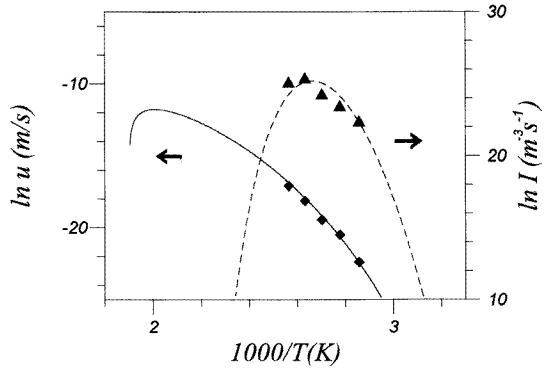

Figure 6. The temperature dependence of the nucleation frequency, I, and the crystal growth, u, for $Se_{85}Te_{15}$ alloy, together with the experimental points from the POM analysis.

The interfacial energy, σ, was assumed to be temperature independent, and its value was estimated from experimentally determined steady-state nucleation rates (Eustathopoulos 1983). In this way a value of $\sigma = 2367 \pm 12$ J mol^{-1} was obtained. According to Turnbull and Cech (1950), the calculated ratios of σ to ΔH_m are fairly constant, ranging from about 1/2 for metallic substances to 1/3 for semimetallic elements (Sb, Bi and Ge). We have found $\sigma/\Delta H_m = 0.358$, in good agreement with the data from the literature.

The values obtained using the previous input parameters from the modelling of the nucleation frequency and crystal growth are plotted as a function of temperature in figure 6. A good agreement with experimental points from optical micrograph analysis is obtained. It is worth remarking that, within the temperature range investigated, the growth rate increases monotonically, whereas the nucleation frequency has a maximum at about 380 K.

4. General discussion

4.1. Activation energies

The activation energies to be considered in a crystallization process are the activation energy for nucleation (E_N), the activation energy for crystal growth (E_G), and that for the whole process of crystallization, called the apparent activation energy and denoted by E_c. The latter is determined from the DSC results. Over a sufficiently limited range of temperature (such as the range of crystallization peaks in DSC experiments), both I and u may be described by an Arrhenius behaviour, and the overall effective activation energy for crystallization can be expressed, according to Yinnon and Uhlmann (1983), as

$$E_c = \frac{E_N + mE_G}{n} \tag{9}$$

where $n = 4$ and $m = 3$, when a constant nucleation frequency, and a tridimensional and isotropic growth exist.

However, in the experimental temperature range of the DSC measurements in continuous-heating experiments (from 385 to 425 K) the nucleation frequency I does not show an Arrhenian behaviour since it rapidly decreases with temperature. This condition can correspond to a quick saturation of nucleation sites. In conclusion, for temperatures not very far from that for the maximum nucleation rate, nucleation phenomena can be neglected and the apparent energy for the whole process of crystallization can be written as

$$E_c \approx E_G. \tag{10}$$

Assuming an Arrhenius behaviour over the temperature range of concern in the DSC study, an activation energy for growth $E_G = 105$ kJ mol^{-1} was found, in good agreement with the activation energy of the overall process found from the DSC measurements, $E_C = 100$ kJ mol^{-1}.

4.2. Crystallization kinetics

Distinct crystallization on the surface and in the bulk of the sample is observed, as is seen in the SEM and POM micrographs. Furthermore, the analyses of the $\ln K_0 f(\alpha)$ versus $\ln(1-\alpha)$ plots shows that there is no single JMAE exponent, n, that describes the whole crystallization process. This means that there are different mechanisms governing the crystallization process that have different weights and degrees of importance depending on the kind of experiment done.

Surface nucleation must overcome a potential barrier lower than that corresponding to bulk nucleation. This means that nucleus formation on the surface will be possible at temperatures lower than those foreseen in the classical nucleation theory. Surface nuclei (or nuclei in other internal breaks or impurities of the material) will appear during the heating before the isothermal temperature is reached or before DSC peaks are seen in non-isothermal conditions (if they did not exist before). These surface nuclei will be called pre-existing nuclei and they will grow with a growth rate given by u. This will determine the kinetics of the mechanism which will be termed surface crystallization.

According to Zanotto (1991) it can be supposed that no new surface nuclei will be formed when the isothermal temperature is achieved. The pre-existing nuclei will grow with a growth rate u, from an average diameter, $\Phi_{\text{pre-ex}}$, and their number, $N_{\text{pre-ex}}$, will remain constant. At the same time, new nuclei will appear in the sample with a frequency rate I. The crystallization originating from these nuclei, which will occur more or less in the terms predicted in the classical nucleation theory, will be termed bulk crystallization.

4.2.1. Surface crystallization kinetics. Germain *et al* (1979) developed a model that describes crystallization kinetics of Ge thin films and explained the different role that is played at every moment by different mechanisms. Among all of the equations in Germain's paper, the most suitable for describing this case is

$$\alpha = \frac{N_{\text{pre-ex}}\pi}{V_0}\left(b^2ut + \frac{2}{3}u^3t^3\right) \tag{11}$$

where V_0 is the total volume of the sample, b a length which defines a crystalline area in the surface of the sample, u the growth rate and t the time. The first term (which is t^1 dependent) corresponds to a kind of growth that the authors call epitaxial-like; it can be interpreted as the growth towards the interior of the sample of a crystalline area on the surface of radius $b \gg \Phi_{\text{pre-ex}}$ (which, in turn, could originate during the growth and subsequent overlap of pre-existing nuclei of diameter $\Phi_{\text{pre-ex}}$ in parts of the sample where their population density is, for some reason, particularly big). The second term (which is t^3 dependent) corresponds to tridimensional growth of isolated semispherical, pre-existing nuclei.

For crystalline fractions $\alpha \leqslant 0.3$, the quantity $-\ln(1-\alpha)$ is well approximated by α. Therefore, in this range of α the exponents accompanying time, t, in equation (11) (1 and 3), can be considered as JMAE exponents, n, and the values inferred from the analyses of the $\ln K_0 f(\alpha)$ versus $-\ln(1-\alpha)$ plots (table 1) compared to them. This description is adequate for describing part of the overall crystallization mechanism. Where JMAE exponents of

the order of 1 appear (especially for $\alpha < 0.3$), it will be possible to say that this surface crystallization mechanism is dominant.

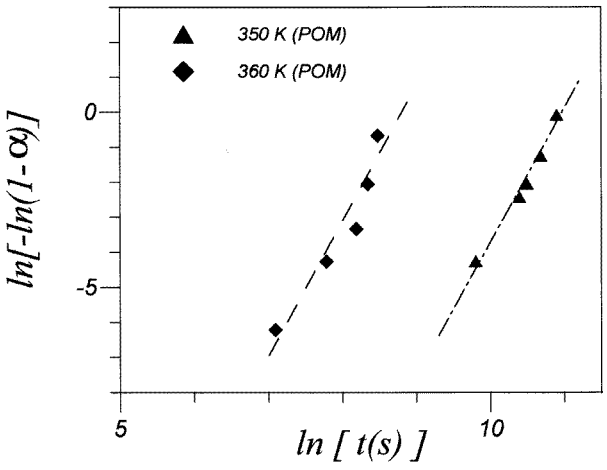

Figure 7. Avrami plots for isothermal heat treatments at 350 and 360 K of the $Se_{85}Te_{15}$ alloy. Full diamonds and full triangles correspond to data determined from the POM analysis.

4.2.2. Bulk crystallization kinetics. The bulk crystallization kinetics will be given by the Avrami equation with an exponent $n = 4$. It has been established, through the determination of α from the POM results, that crystallization in the bulk of the sample follows this kind of kinetics (figure 7). This mechanism would be dominant at times for which Iu^3t^4 (which is the term that governs the bulk crystallization mechanism) has more importance than the corresponding term for the surface crystallization mechanism. However, it is expected that, in the initial stages of the transformation, the surface crystallization term would be more important and, only when crystallization advances enough, the bulk crystallization term is dominant (especially in samples with a low surface/bulk relationship, i.e. bulk samples), leading to high JMAE exponents (near 4).

4.2.3. Overall kinetics. In the overall crystallization kinetics there will be competition between the two mechanisms explained above. It will be seen that different ways of crystallizing the sample lead to different results for the overall kinetics. Four cases are considered.

(i) Isothermal experiments at temperatures well below $T = 380$ K (the temperature for the maximum of the nucleation frequency): No 1 and No 2. In these experiments the surface crystallization mechanism is dominant through the whole transformation. The reason for this behaviour is that, for these temperatures, I is one or two orders of magnitude below its maximum value, and the number of newly generated nuclei is not enough for the bulk crystallization mechanism to become significant.

(ii) Isothermal experiments at temperatures near $T = 380$ K: No 3 and No 4. For these experiments surface crystallization is dominant at the initial stages of the transformation. During its course bulk crystallization becomes dominant, and JMAE exponents of $n = 4$ are achieved.

(iii) Non-isothermal experiments for $0.625 \leqslant \beta \leqslant 1.25$ (β in K min^{-1}). In these experiments we obtain the same crystallization kinetics as in the isothermal experiments No 3 and No 4. The reason for this being so is that the range of temperature in which the transformation takes place includes the temperature at which I reaches its maximum value. Therefore, it is expected that bulk crystallization will play an important role.

(iv) Non-isothermal experiments for $2.5 \leqslant \beta \leqslant 20$ (β in K min^{-1}). In this case, bulk crystallization never becomes dominant (this can be seen from the fact that the maximum JMAE exponent is $n = 3$). For all of these heating rates the transformation temperatures are above $T = 380$ K. As the nucleation frequency decreases dramatically with temperature after 380 K, crystallization proceeds via the surface mechanism.

4.3. Predictions of the model and a comparison with experimental data

For a polymorphous phase transformation, given nucleation and growth rates, it is possible to derive the time–temperature–transformation (T–T–T) curves which relate the time and the temperature required to produce specific volume fractions, α, of crystals. This is achieved through the Avrami equation (Avrami 1939, 1940, 1941), which relates α to the nucleation frequency, I, growth rate, u, and time, t:

$$\alpha = 1 - \exp\left(-\frac{w I u^m}{m+1}(t-\tau)^{m+1}\right) \tag{12}$$

where $n = m + 1$ is the JMAE exponent and τ is the transient time, and, at any given temperature, I and u are constant.

Table 3. The temperature dependence of the experimental induction period (τ) and time (τ_u) required for growth to a visible size.

T (K)	τ (s)	$\tau_u = L/u$ (s)
350	2700	2631
360	330	400
370	182	138
380	20	37
390	—	13

In order to discuss whether or not the experimental induction period τ can be neglected, a qualitative approach was adopted (Gutzow *et al* 1978) and it was assumed that τ includes both a non-stationary time lag, τ_0, and the time τ_1 required for the appearance of the first nucleus, as well as the time τ_u required for growth of the nucleus from the Gibbs–Thomson size to a size, L, visible under the optical microscope, i.e.,

$$\tau \approx \tau_0 + \tau_1 + \tau_u. \tag{13}$$

The order of magnitude of τ_u can be evaluated as $\tau_u \approx L/u$, where u is the growth rate at a given temperature and L is the minimum size visible under the optical microscope. In our working conditions, $L \approx 0.5$ μm, and τ_u-values comparable to the intercept on the time axis of the N_v versus t plots are obtained, as can be seen in table 3, where a comparison of time intercepts and calculated values of τ_u is presented. Thus the transient time found in this work has its main origin in the experimental method used; however, induction times τ_0 or τ_1 could exist, but they would be so short that they can be neglected.

The experimental results from POM show that isotropic growth occurs and that the nucleation frequency and growth rate may be considered as constant at any given temperature

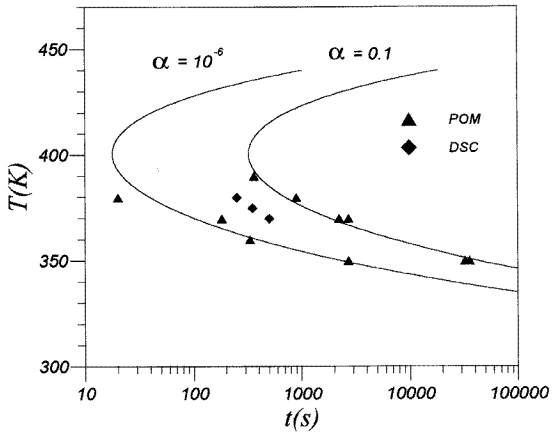

Figure 8. T–T–T curves corresponding to crystalline fractions of $\alpha = 10^{-6}$ and 0.1, with experimental points from optical micrograph ($\alpha = 10^{-6}$ and 0.1, full triangles) and DSC ($\alpha = 0.1$, full diamonds) analysis.

throughout the crystallization for this alloy. For this reason, the Avrami equation with an exponent $m = 3$ is used. The T–T–T curves are thus calculated and the results are shown in figure 8. These are compared with the experimental data from both POM and DSC analysis. Since POM results are determined for the bulk crystallization, good agreement between the experimental points and the calculated curves is an indication that equation (12) correctly describes the bulk crystallization kinetics. On the other hand, DSC results represent the overall crystallization, and so it is expected that large discrepancies will be observed, according to what has been discussed previously.

5. Conclusions

The crystallization kinetics of a $Se_{85}Te_{15}$ glassy alloy obtained by air quenching has been determined through the use of POM and DSC. The samples have been structurally characterized by SEM and XRD.

The values and temperature dependence of the nucleation frequency, I, and the growth rate, u, have been evaluated by means of POM and the classical nucleation and normal growth theories, respectively. The values predicted are in excellent agreement with direct observations and they allow us to justify the value of the apparent activation energy, E_c, and the relative importance, for different heat treatments, of the distinct crystallization mechanisms that have been identified: bulk and surface crystallization. For the bulk crystallization mechanism the kinetics has been satisfactorily determined. It fits to the JMAE model with an exponent $n = 4$. The T–T–T curves have been calculated with the Avrami equation ($m = 3$) and show a good fit to POM results (which represent bulk crystallization) and a poor one to DSC results (which represent the overall crystallization). It is also possible to fit the overall crystallization kinetics to the same model, though different values of the JMAE exponent, n, are required to reproduce the behaviour over the whole range of transformed fractions. This is due to the existence of surface crystallization. A simple model has been presented, which seems to describe approximately this part of the crystallization kinetics. The parameters on which the model depends provide us with an indication of how difficult is to control the crystallization originating via this mechanism for the samples of $Se_{85}Te_{15}$ studied.

References

Abdel-Rahim M A 1992 *J. Mater. Sci.* **27** 1757
Avrami M 1939 *J. Chem. Phys.* **7** 1103
——1940 *J. Chem. Phys.* **8** 212
——1941 *J. Chem. Phys.* **9** 177
Afify N 1991 *J. Non-Cryst. Solids* **128** 279
——1992 *J. Non-Cryst. Solids* **142** 247
Baró M D, Calventus Y, Suriñach S, Clavaguera-Mora M T and Clavaguera N 1992 *Trends in Non-Crystalline Solids* ed A Conde, C F Conde and M Millán (Singapore: World Scientific) p 193
Baró M D, Suriñach S, Malagelada J, Clavaguera-Mora M T, Gialanella S and Cahn R W 1993 *Acta Metall. Mater.* **41** 1065
Bordas S 1977 *PhD Thesis* UPB
Cahn J W and Nutting J 1959 *Trans. Metall. Soc. AIME* **215** 526
Calventus Y 1994 *PhD Thesis* UAB
Das G C, Bever M B and Uhlmann D R 1972 *J. Non-Cryst. Solids* **7** 251
Eustathopoulos N 1983 *Int. Met. Rev.* **28** 189
Faivre G and Gardissat J L 1986 *Macromolecules* **19** 1988
Germain P, Zellama K, Squelard S and Bourgoin J C 1979 *J. Appl. Phys.* **50** 6986
Grison E 1951 *J. Chem. Phys.* **19** 1109
Ghosh G, Lukas H L and Delaey L 1988 *Calphad* **12** 295
Gutzow I, Dochev V, Pancheva E and Dimov K 1978 *J. Polym. Sci.* **6** 1155
Kissinger H E 1957 *Anal. Chem.* **29** 1702
Kotkata M F, Mahmoud E A and El-Mously 1981 *Acta Phys. Acad. Sci. Hungaricae* **50** 61
Mehra R M, Kaur G, Pundir A and Mathur P C 1993 *Japan. J. Appl. Phys.* **32** 128
Miyanaga T, Crozier E D, Seary A J, Cutler M and Bell F G 1993 *Japan. J. Appl. Phys.* **32** 700
Ranganathan S and von Heimendahl M 1981 *J. Mater. Sci.* **16** 2401
Rialland J F and Perron J C 1976 *Proc. 7th Conf. on Amorphous and Liquid Semiconductors* p 371
Suriñach S, Baró M D, Clavaguera-Mora M T and Clavaguera N 1983 *J. Non-Cryst. Solids* **58** 209
Tamura K, Inui M, Yao M, Endo H, Hosokawa S, Hoshino H, Katayama Y and Maruyama K 1991 *J. Phys.: Condens. Matter* **3** 7495
Thompson C V and Spaepen F 1979 *Acta Metall.* **27** 1855
Turnbull D and Cech R E 1950 *J. Appl. Phys.* **21** 804
Venugopal Reddy K and Bhatnagar A K 1992 *J. Phys. D: Appl. Phys.* **25** 1810
Ward A T 1970 *J. Chem. Phys.* **74** 4110
Yang H, Wang W and Ming S 1986 *J. Non-Cryst. Solids* **80** 503
Yinnon H and Uhlmann D R 1983 *J. Non-Cryst. Solids* **54** 253
Zanotto E D 1991 *J. Non-Cryst. Solids* **129** 183